

1996 ACTIVITIES

INTRODUCTION

In 1996, GRD scientists focused their study on atmospheric chemistry, biogeochemical oceanography, and environmental radioactivity.

International/National scientific programs and budgetary funds for our studies are shown in Table 2.

I. Field Observation Studies

GREENHOUSE GASES (CO₂, CH₄, and CO)

1. Studies on Greenhouse Gases in Upper Air Using Commercial Airliners

1.1 Atmospheric CO₂ and CH₄ measurements from 1993 to 1994

Matsueda and Inoue (1996)

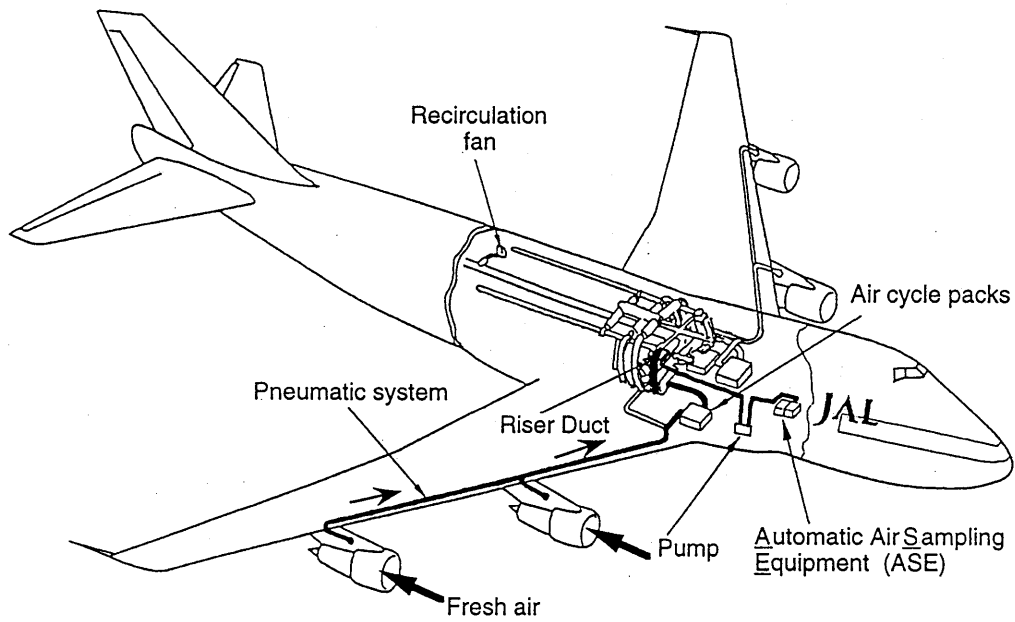
The increase of trace gases such as carbon dioxide in the atmosphere is expected to contribute to on-going global warming and to affect the chemical cycles in the atmosphere. Recent levels of greenhouse gases in surface air have been regularly observed at worldwide sampling networks such as NOAA/CMDL and GAW, but few systematic measurements have been made of greenhouse gases in the upper atmosphere.

Matsueda and Inoue (1996) developed a new automatic flask sampling system for the Boeing 747 commercial airliner in April 1993 to observe the mixing ratios of CO₂, CH₄ and other trace gases in the upper atmosphere at altitudes of 9–13 km using regular commercial flights between Australia and Japan. This program was to clarify seasonal variations and secular trends in greenhouse gases in the upper atmosphere through cooperation supported by the JAL Foundation, Japan Airlines (JAL), the JMA, and Japan's Ministry of Transportation.

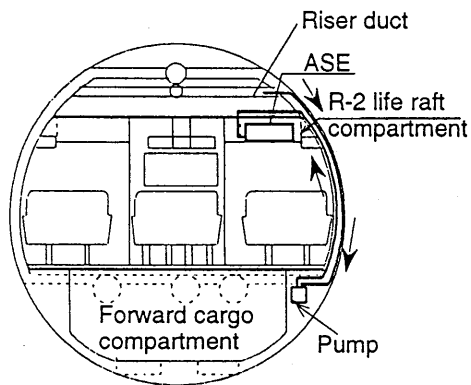
They described their sampling system and the results of CO₂ and CH₄ measurements in the upper troposphere for one year from 1993 to 1994 (Fig. 96-1). The air sampling system was developed to collect air samples automatically in 12 electrochemically buffed titanium flasks of automatic air sampling equipment (ASE) using a metal bellows pump. Engine bleed (fresh air outside the aircraft) was introduced into the ASE through a pneumatic system and a bypass intake using a metal bellows pump for flushing and compressing the air sample into flasks. Storage tests indicated no significant change of CO₂ and CH₄ mixing ratios in sample flask until analysis.

The air sample was analyzed for the CO₂ mixing ratio using an NDIR and for CH₄ mixing ratio using a GC-FID in the laboratory. Analytical precision for measurement was less than ± 0.02 ppm for CO₂ and less than $\pm 0.12\%$ for CH₄.

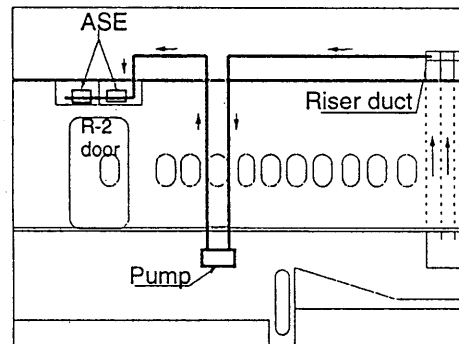
The CO₂ and CH₄ mixing ratios in the air sample were referenced to five working standard gases of CO₂ in air and CH₄ in air. Working standards were calibrated regularly by primary standards. No significant drift of mixing ratio was found in any of the working standards in high-pressure aluminum cylinders for one year. All mixing ratios are reported in ppm or ppb by mole fraction in dry air based on the WMO x85 scale for CO₂ and the MRI/GRD scale for CH₄.



(a) Bird's-eye view



(b) Rear view



(c) Side view

Fig. 96-1 Air flow diagrams of flask sampling system developed for Boeing 747 commercial airliner. Bold lines indicate sample airstream in the aircraft by bird's-eye view (a), rear view (b), and side view (c). Reprinted from *Atmospheric Environment*, 30, Matsueda and Inoue, Measurements of atmospheric CO₂ and CH₄ using a commercial airliner from 1993 to 1994, 1647-1655, Copyright (1996), with kind permission from Elsevier Science.

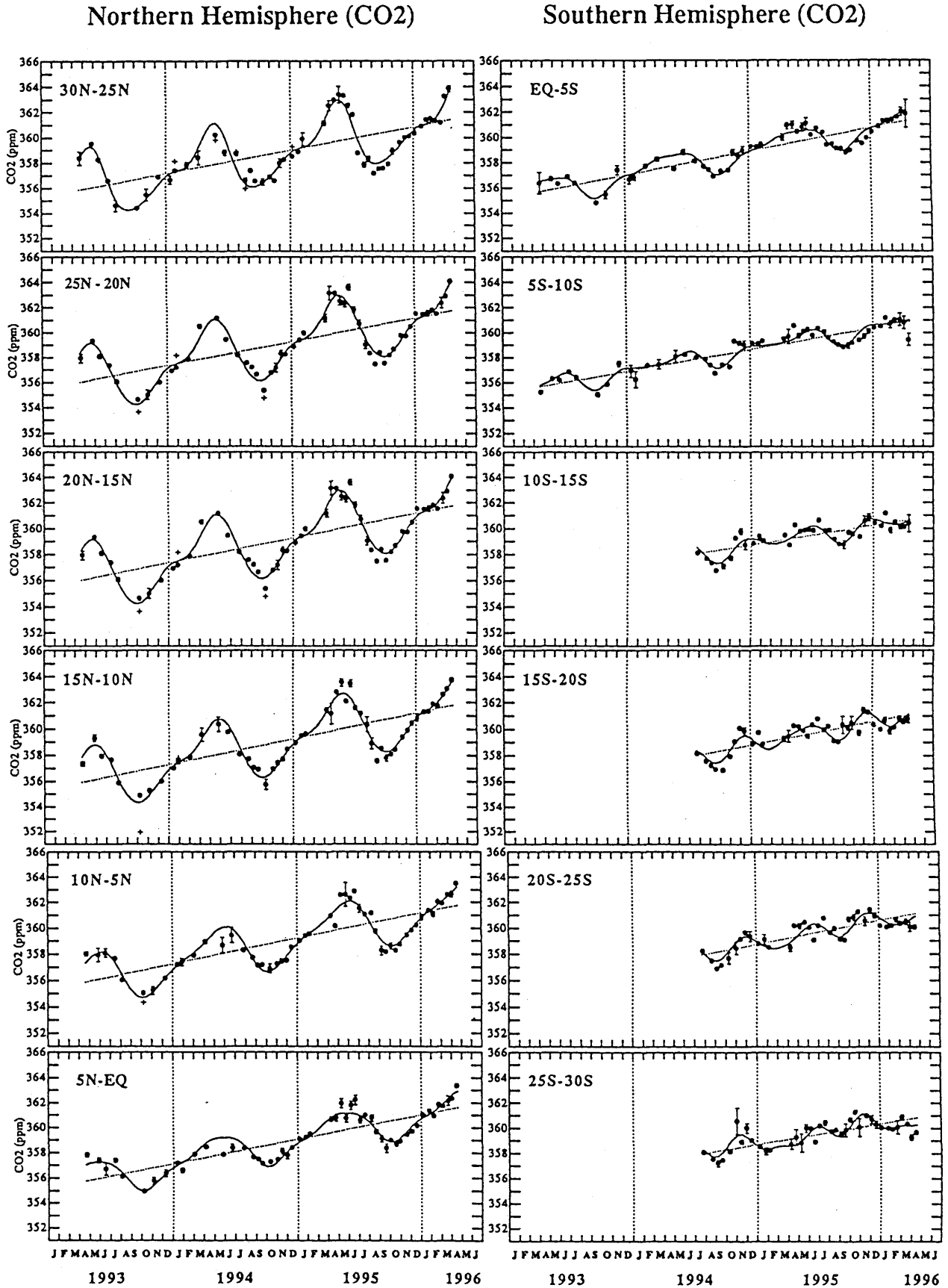


Fig. 96-2 Averaged CO₂ mixing ratios (closed circles) and SD (error bars) for 12 latitudinal bands between 30°N and 30°S at 9-13 km over western Pacific. Selected data presented as (+). Thick lines: best fit curve of data; dotted lines: fitted straight trend.

Northern Hemisphere (CH₄)

Southern Hemisphere (CH₄)

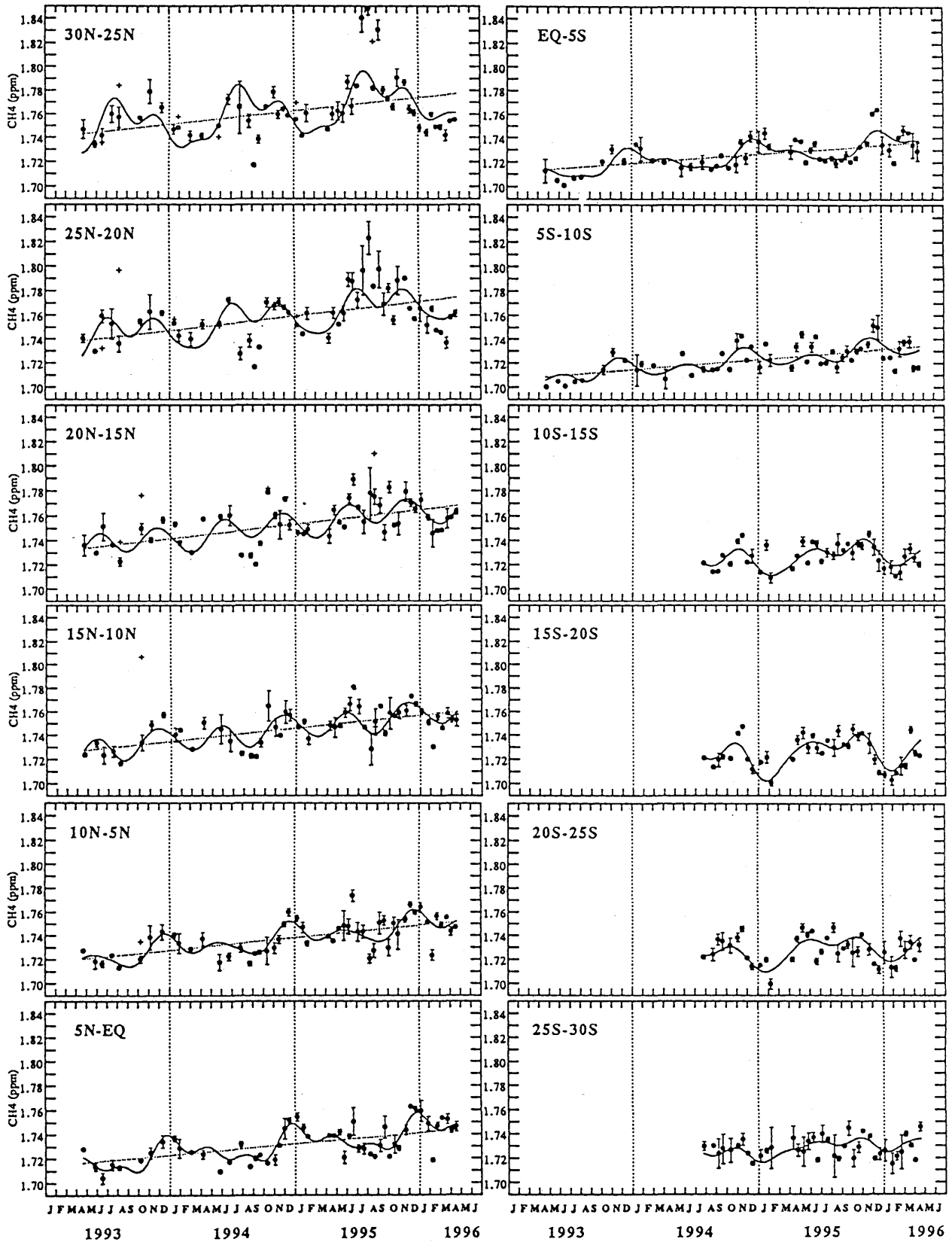


Fig. 96-3 As in Fig. 96-2 for CH₄.

Air was sampled monthly over the western North Pacific between Narita (35°46'N, 140°23'E), Japan, and Cairns, (16°53'S, 145°45'E), Australia, during 1993-1994 (Figs. 1 and 2). Measurements of CO₂ and CH₄ in the Northern Hemisphere showed a clear seasonal cycle greatly influenced by the seasonal variation in the lower troposphere (Figs. 96-2 and 96-3). A significant decrease in mixing ratio during winter was observed in CH₄ variation, suggesting the intrusion of lower stratospheric air into the upper troposphere. The seasonal variation of both gases gradually decayed toward the equator, but a different seasonal cycle appeared in the Southern Hemisphere. This change indicated the significance of meridional transport of both gases through the upper troposphere into the Southern Hemisphere. The mixing ratio level of both gases showed a recent increase in the upper troposphere.

1.2 CO₂, CH₄, and CO in the upper troposphere from 1993 to 1996

Matsueda, Inoue, and Ishii (1997)

Matsueda *et al.* (1997) summarized observation results for CO₂, CH₄ and CO in the upper troposphere observed using a commercial airliner from 1993 to 1996. To expand the observation region to the south, sampling flights after July 1994 were made using a different JAL airliner from Sydney (16°53'S, 145°45'E) to Narita, Japan. Sampling flight frequency was increased to about twice a month to obtain higher time resolution data.

The sampling system was operated regularly using a JAL airliner between Australia and Japan for 3 years from April 1993 to April 1996. A unique set of data for trace gases has been obtained in the upper troposphere at 9-13 km over the western Pacific. Data analysis of the observed results indicated they were successful in observing recent trends and seasonal cycles of CO₂, CH₄, and CO between 30°N and 30°S (Figs. 96-2, 96-3 and 96-4). The recent trend indicated recovery in the rate of CO₂ and CH₄ increase after the great anomaly around 1992. Seasonal cycles showed a large difference between the Northern and Southern Hemispheres. The northern seasonal cycle was influenced by lower tropospheric variations and mixing processes in stratospheric air, while upper tropospheric transport was identified as an important process for the seasonal cycle in the Southern Hemisphere. In addition, biomass burning in the Southern Hemisphere was identified as an additional source of trace gases in the upper troposphere.

More long-term observation is necessary in this program to gain a better understanding of the global cycle of trace gases in the upper troposphere. Special attention should be paid to the impact of widespread biomass burning on the upper atmospheric environment.

Northern Hemisphere (CO)

Southern Hemisphere (CO)

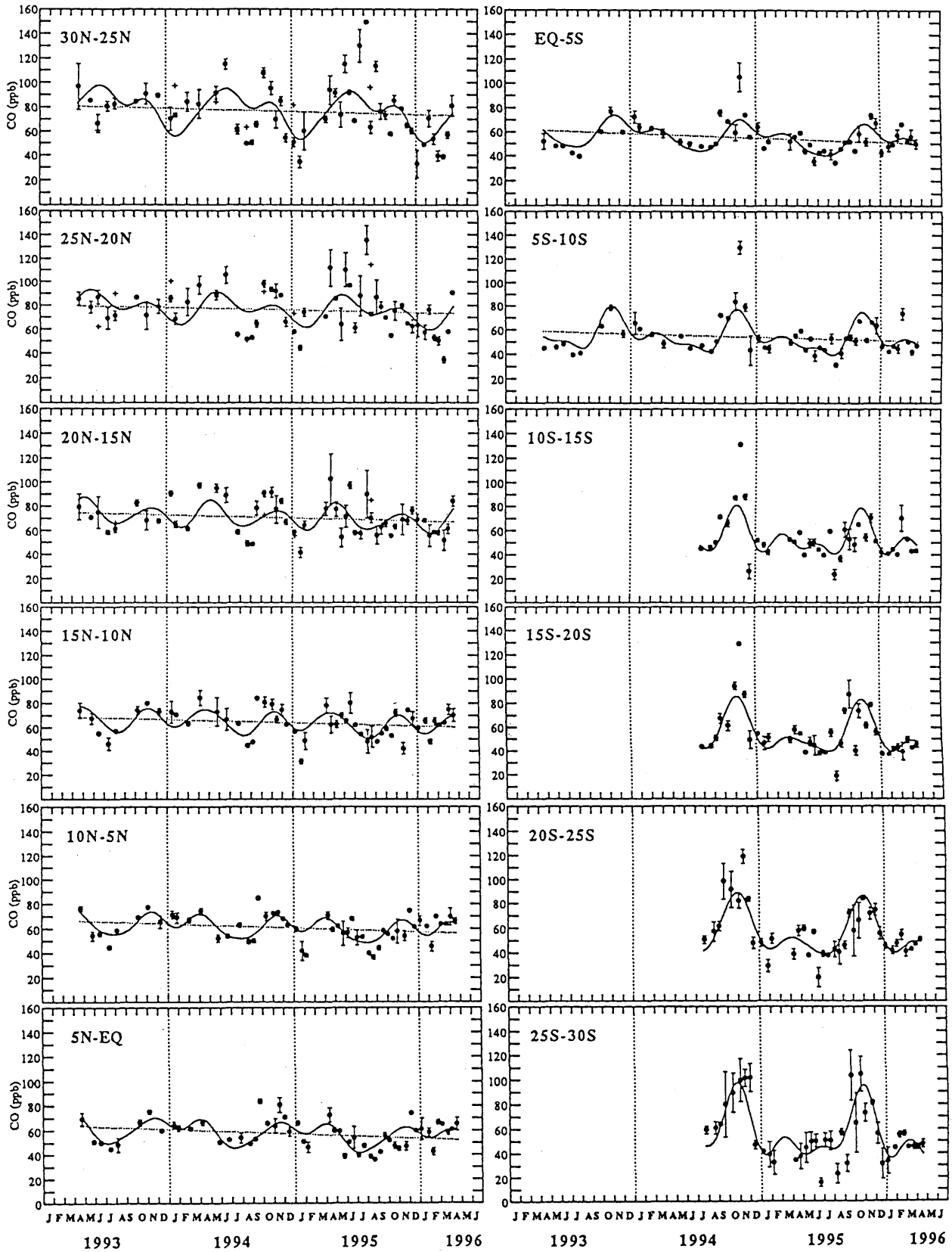


Fig. 96-4 As in Fig. 96-2 for CO.

2. Greenhouse Gas Behavior in Western and Central Pacific Ocean

2.1 Evaluation of CO₂ exchange at sea surface in western North Pacific: ΔpCO₂ distribution and CO₂ flux

Murata, Fushimi, Inoue, Hirota, Nemoto, Okabe, Yabuki, and Asanuma (1996)

We conducted repeated observation of carbon dioxide partial pressure (pCO₂) in the western North Pacific since 1981. The increasing trend of pCO₂ in surface water in the region north of 10°N at 137°E was reported for the first time by Inoue *et al.* (1995) as described in 1995 ACTIVITIES. This result suggests that the middle latitude of the western North Pacific is a sink for atmospheric CO₂ and pCO₂ is increasing.

To evaluate CO₂ exchange at the sea surface in the western North Pacific (130°E-160°E, 30°N-0°) throughout one year, Murata *et al.* (1996) mapped the ΔpCO₂ using data observed from 1987 to 1993 by the JMA and the MRI on board several research vessels (Fig. 96-5). They calculated the CO₂ flux based on surface seawater CO₂ normalized, interpolated, and extrapolated using the temperature dependence of dissolved CO₂ determined empirically (Fig. 96-6).

They obtained the following results:

- (1) The ΔpCO₂ map shows that the region north of 10°N is a sink of <-70 μatm at a maximum in winter and a source of >40 μatm at a maximum in summer. This demonstrates a large seasonal change in ΔpCO₂ reaching 90 μatm.
- (2) The region south of 10°N is a source of 40 μatm in winter and is almost at equilibrium with atmospheric CO₂ in summer. This seasonal tendency is the reverse of that in the region north of 10°N.
- (3) Integrated annual net CO₂ flux is -22.4/-48.6 MtC (ocean influx) in the region north of 10°N and 3.7/5.4 MtC (ocean efflux) south of it, depending on the wind-dependent transfer velocity and exchange coefficient (Table 96-1).

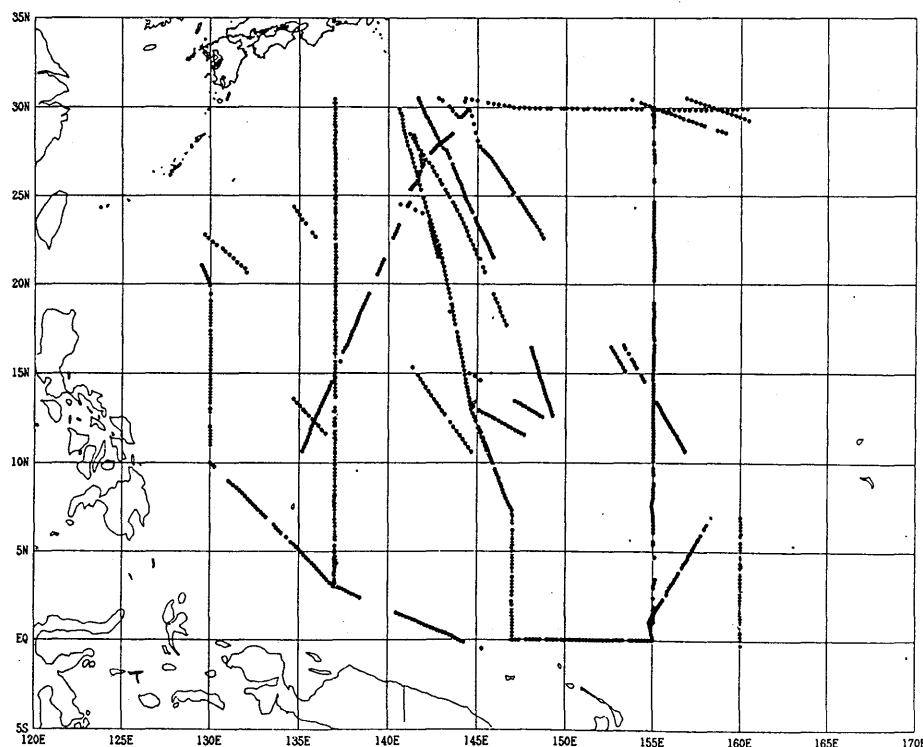
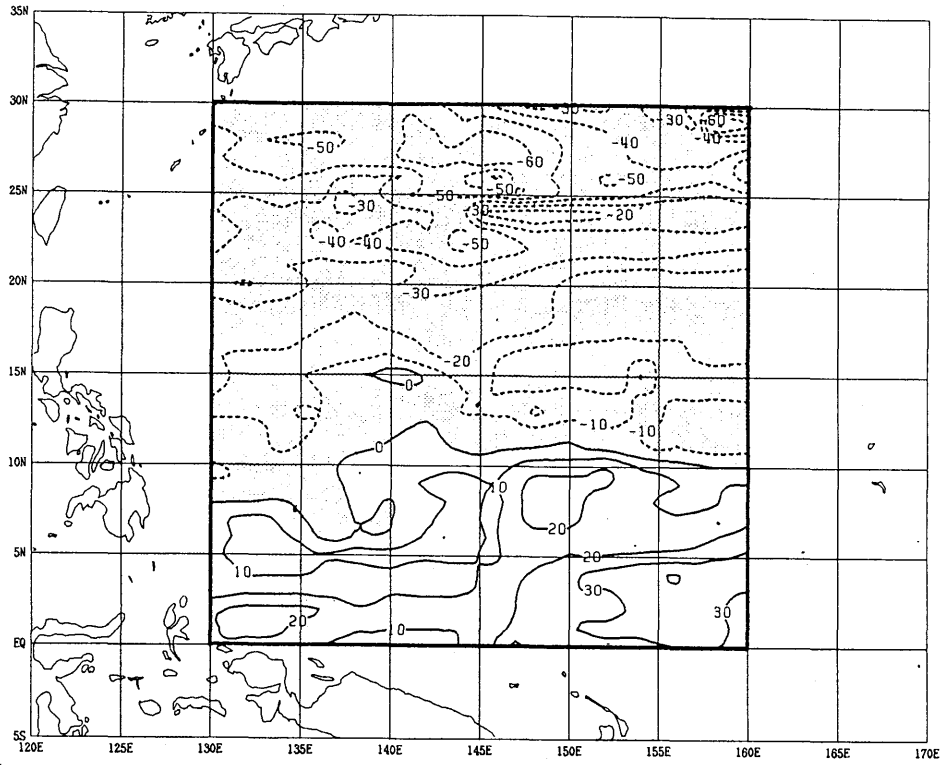


Fig. 96-5 Surface seawater CO₂ data points observed from 1987 to 1993 by JMA and MRI.

$\Delta p\text{CO}_2$ (μatm): January



$\Delta p\text{CO}_2$ (μatm): February

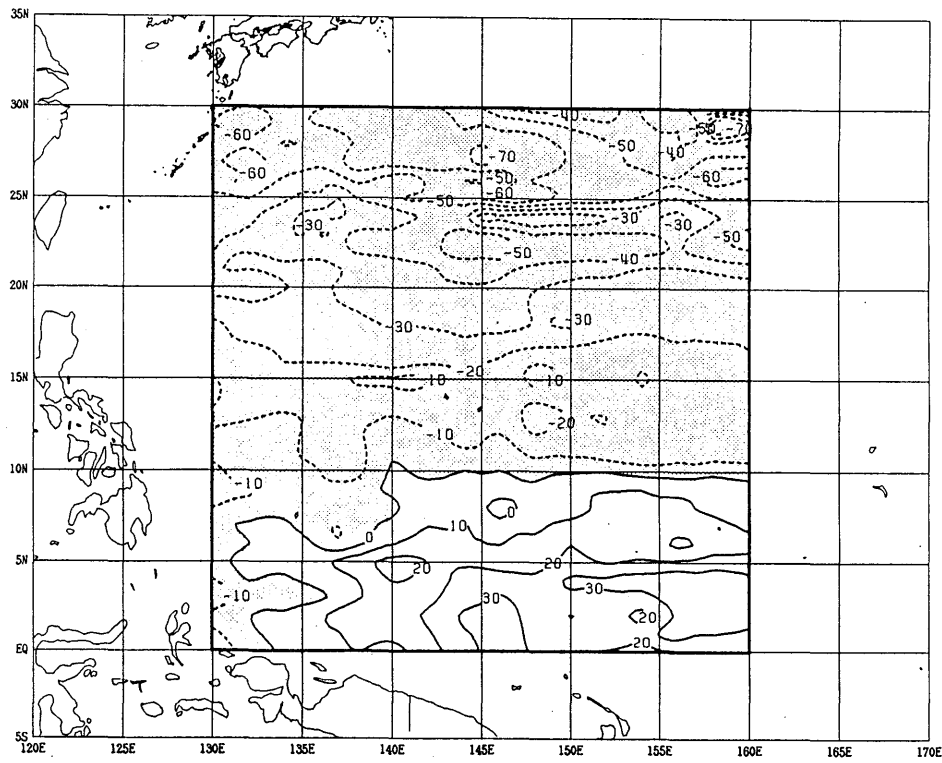
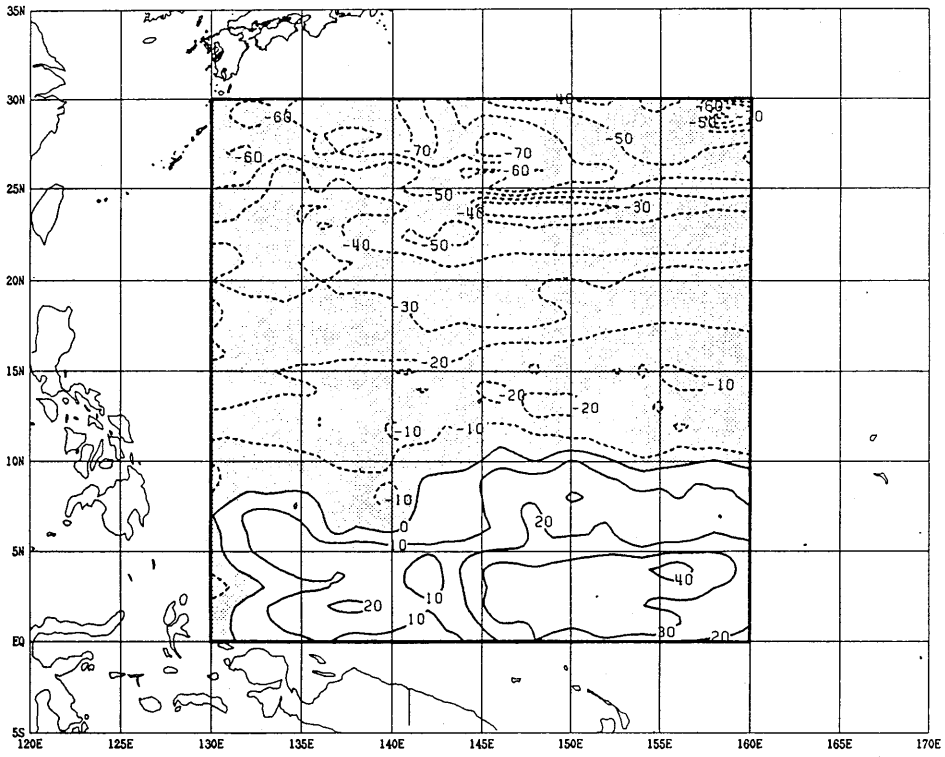


Fig. 96-6 Distribution of reconstructed $\Delta p\text{CO}_2$ (μatm) from January to December 1990. The dotted pattern indicates negative (air-to-sea) $\Delta p\text{CO}_2$.

$\Delta p\text{CO}_2$ (μatm): March



$\Delta p\text{CO}_2$ (μatm): April

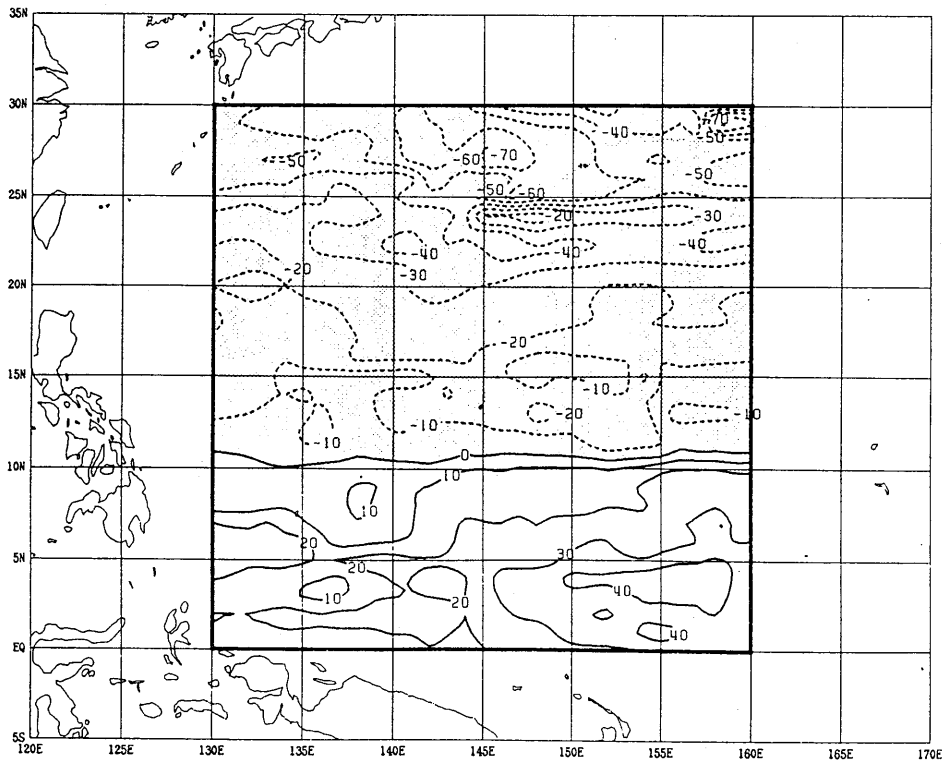
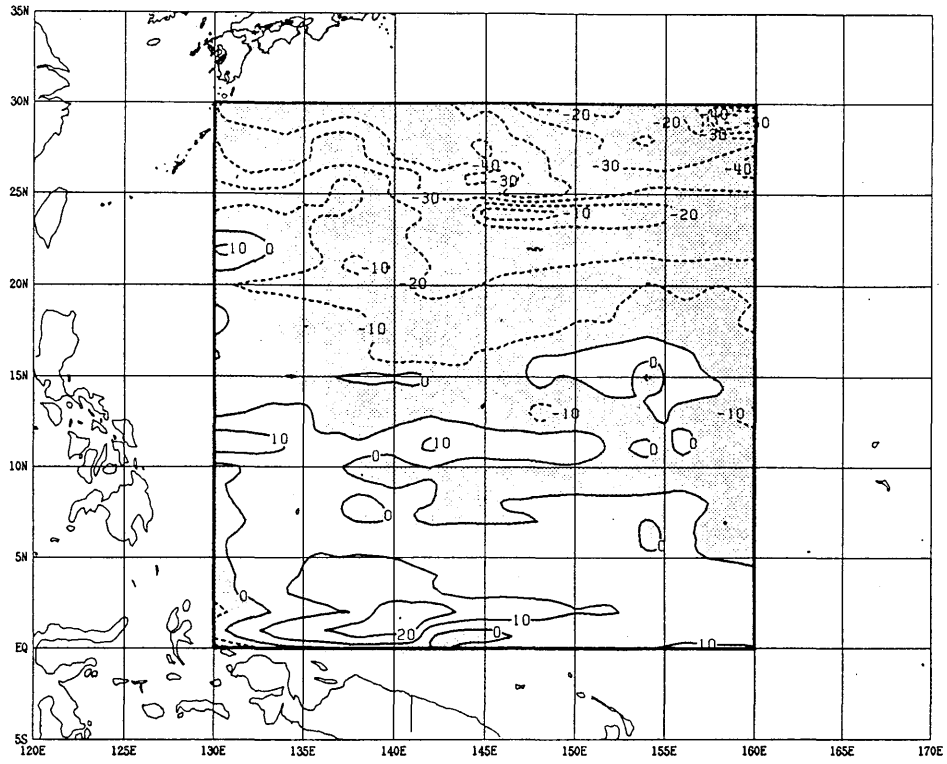


Fig. 96-6 Continued.

$\Delta p\text{CO}_2$ (μatm): May



$\Delta p\text{CO}_2$ (μatm): June

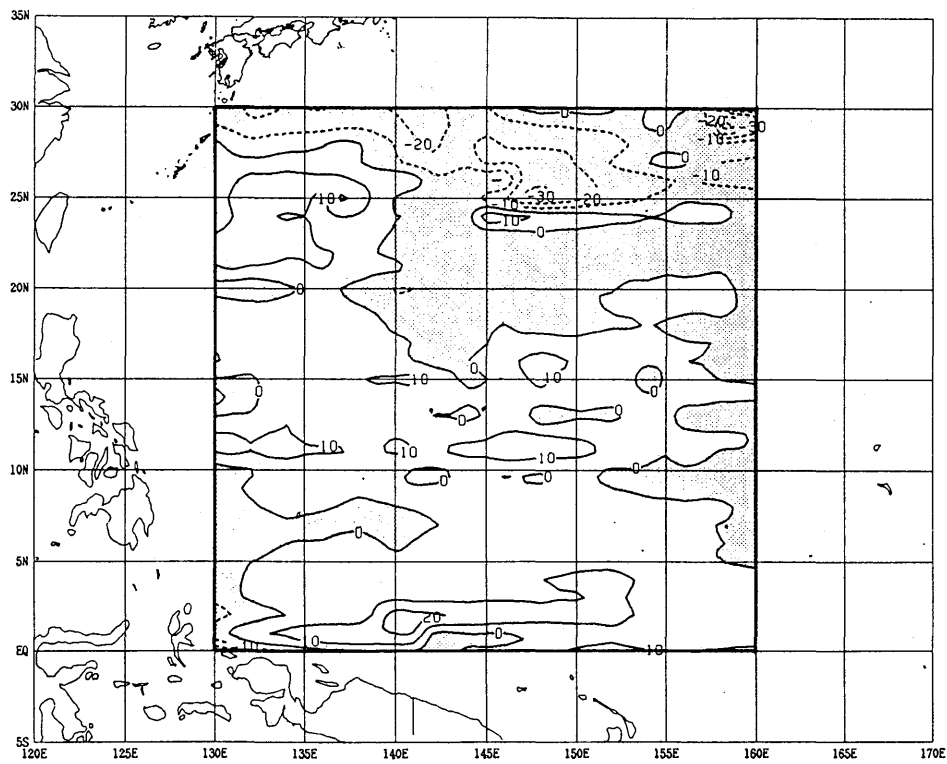
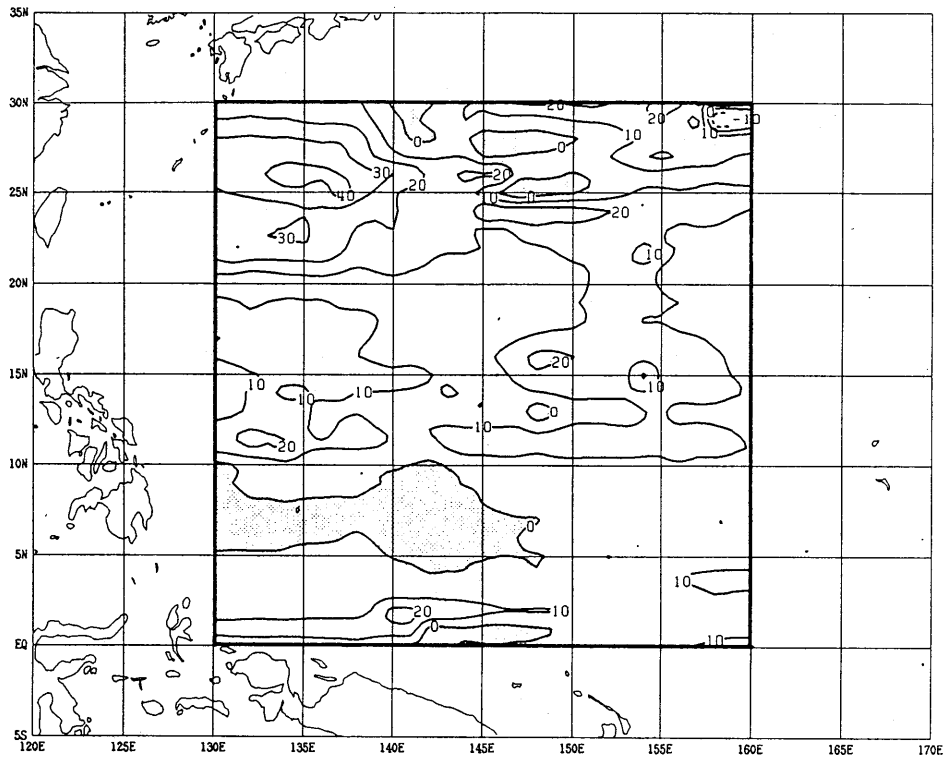


Fig. 96-6 Continued.

$\Delta p\text{CO}_2$ (μatm): July



$\Delta p\text{CO}_2$ (μatm): August

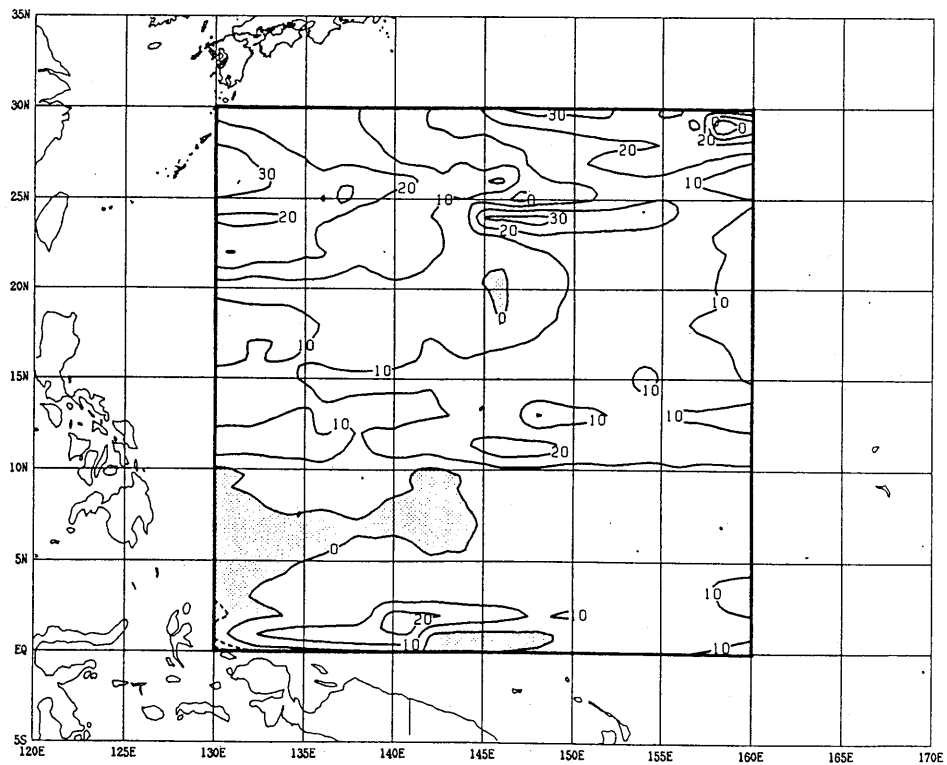
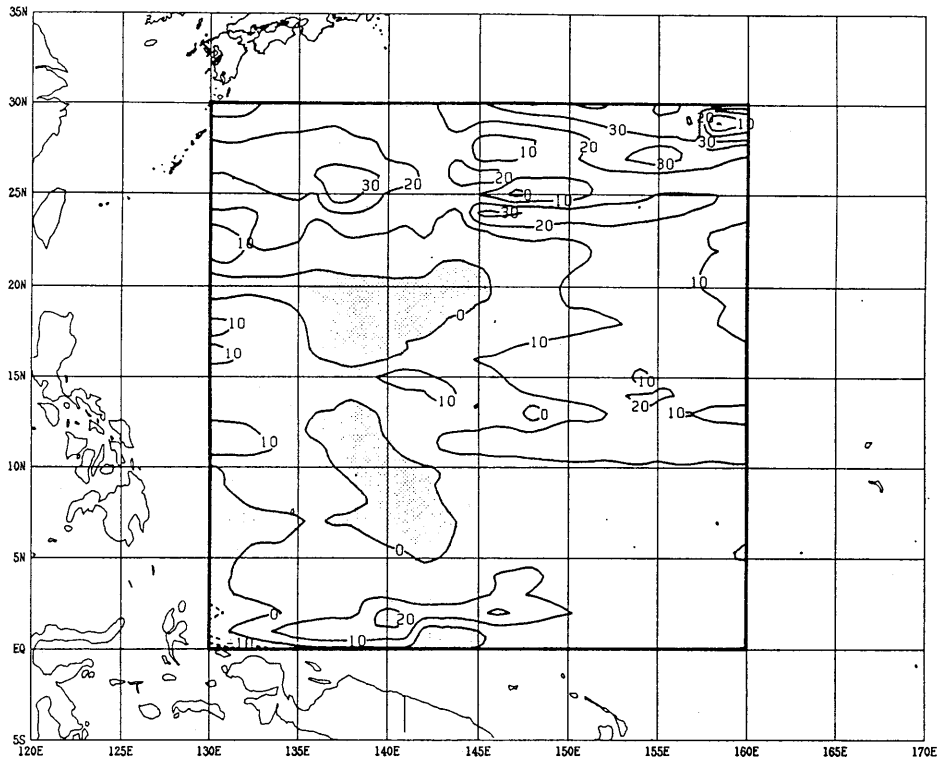


Fig. 96-6 Continued.

ΔpCO_2 (μatm): September



ΔpCO_2 (μatm): October

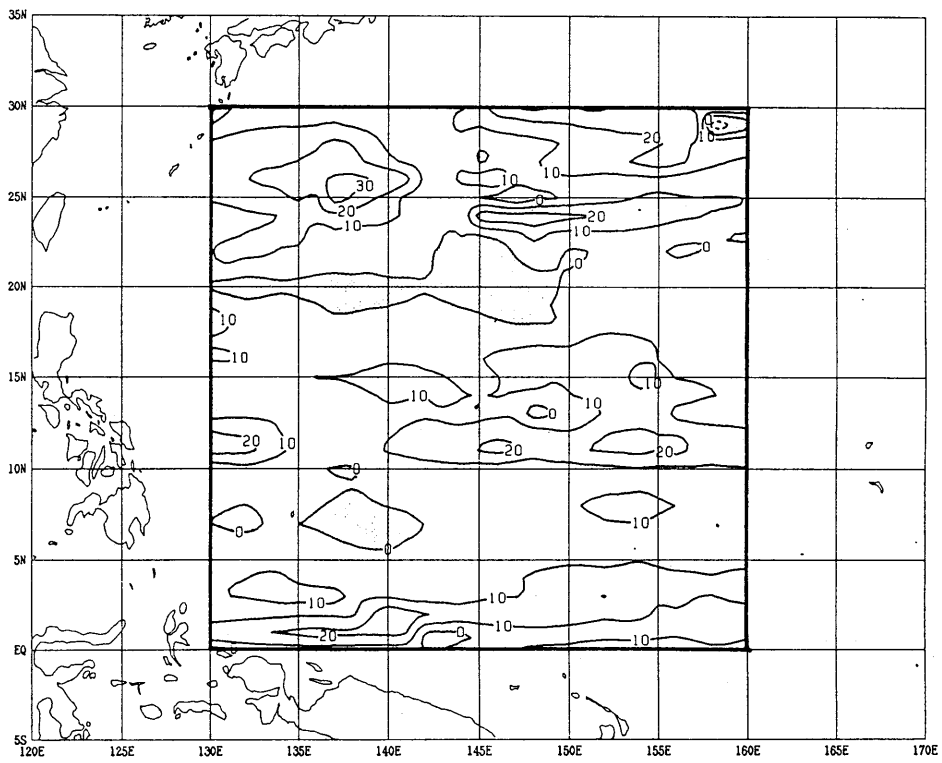
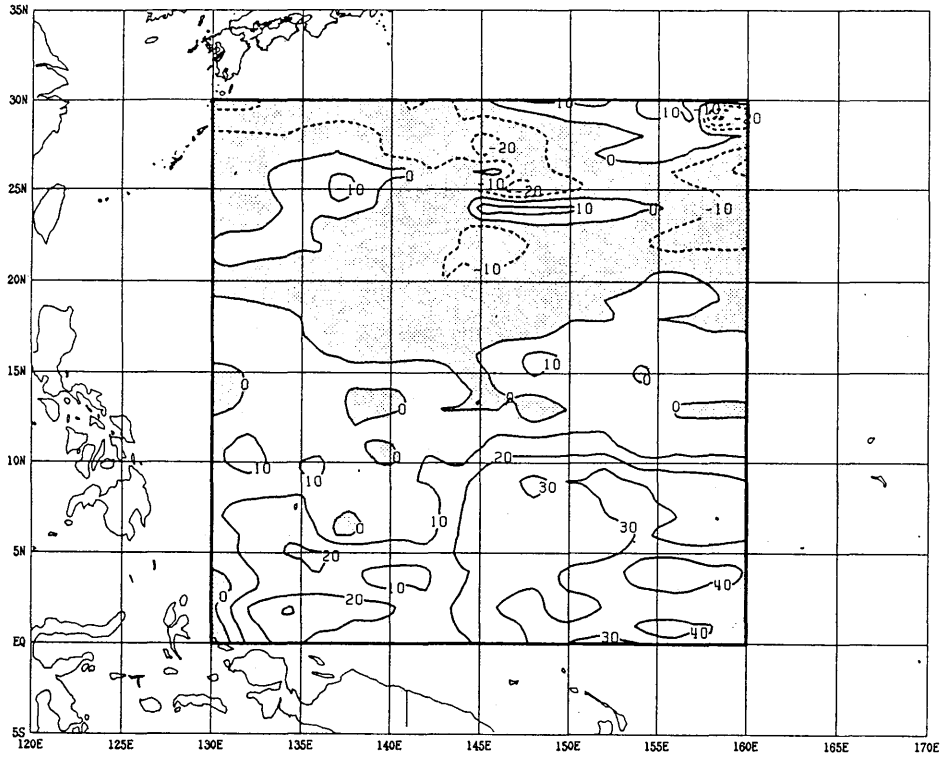


Fig. 96-6 Continued.

$\Delta p\text{CO}_2$ (μatm): November



$\Delta p\text{CO}_2$ (μatm): December

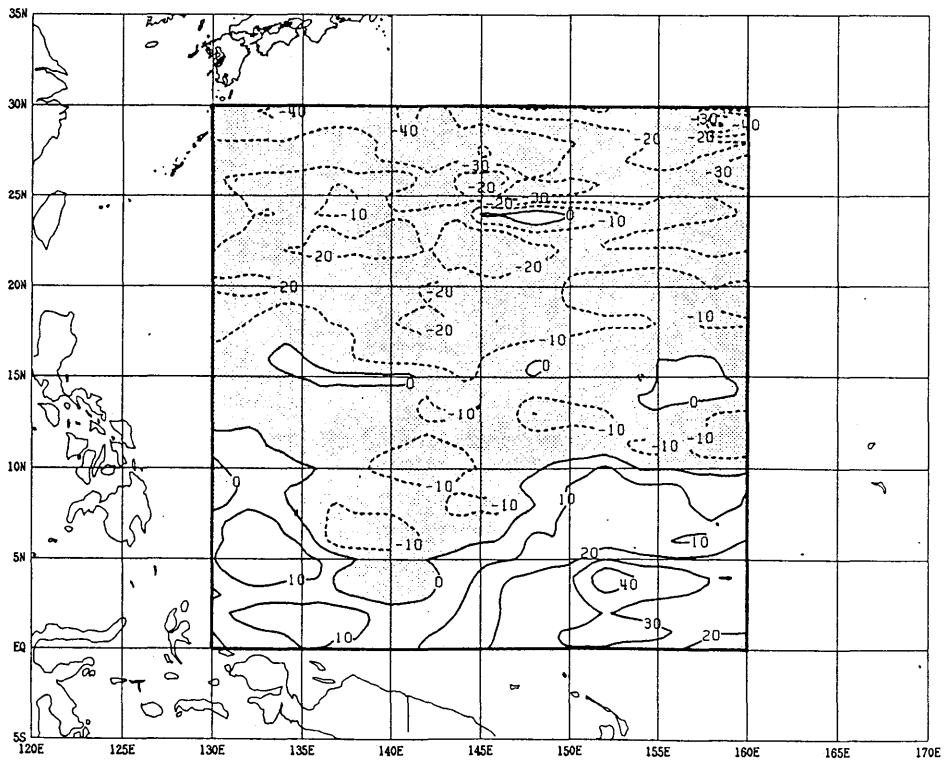


Fig. 96-6 Continued.

Table 96-1 Estimates of sea-to-air CO₂ flux (Mt of C) in the regions north and south of 10°N for each month, separated for (a) LM and (b) TFT formula.

(a)													
	J	F	M	A	M	J	J	A	S	O	N	D	Total
> 10°N	-7.2	-5.6	-6.3	-4.0	-2.1	0.0	1.2	2.6	1.9	1.3	-0.5	-3.5	-22.4
≤ 10°N	0.6	0.3	0.3	0.3	0.1	0.2	0.0	0.1	0.1	0.1	1.3	0.3	3.7

(b)													
	J	F	M	A	M	J	J	A	S	O	N	D	Total
> 10°N	-15.1	-12.3	-13.4	-8.7	-4.7	0.0	2.3	5.2	3.9	2.7	-1.1	-7.3	-48.6
≤ 10°N	1.1	0.6	0.3	0.4	0.0	0.2	0.0	0.1	0.1	0.1	2.1	0.3	5.4

2.2 Changes in longitudinal distribution of CO₂ partial pressure in central and western equatorial Pacific, west of 160°W

Inoue, Ishii, Matsueda, Aoyama, and Asanuma (1996)

We focused our study on pCO₂ distribution variation in the western and central equatorial Pacific with relation to El Niño/Southern Oscillation (ENSO) phenomena. The equatorial Pacific is known as a strong oceanic source of atmospheric CO₂. CO₂ is supplied to the atmosphere mostly in the eastern and central equatorial Pacific due to upwelling containing CO₂-rich water.

Inoue *et al.* (1996) described spatial and temporal variations in pCO₂ in the central and western equatorial Pacific based on measurements conducted between 1987 and 1994. Surface water pCO₂ data indicate significant differences in longitudinal distribution depending on ocean conditions (Figs. 96-7 and 96-8). They examined the relationship between the area showing higher surface pCO₂ and ENSO phenomena by using the Southern Oscillation Index (SOI) (Fig. 96-9). Results indicate that the area showing higher surface pCO₂ correlates with the SOI, and the western edge of the higher pCO₂ area moves eastward with increasing SOI, which suggests significant intra- and interannual fluctuations of CO₂ outflux from the central and western equatorial Pacific (Fig. 96-10).

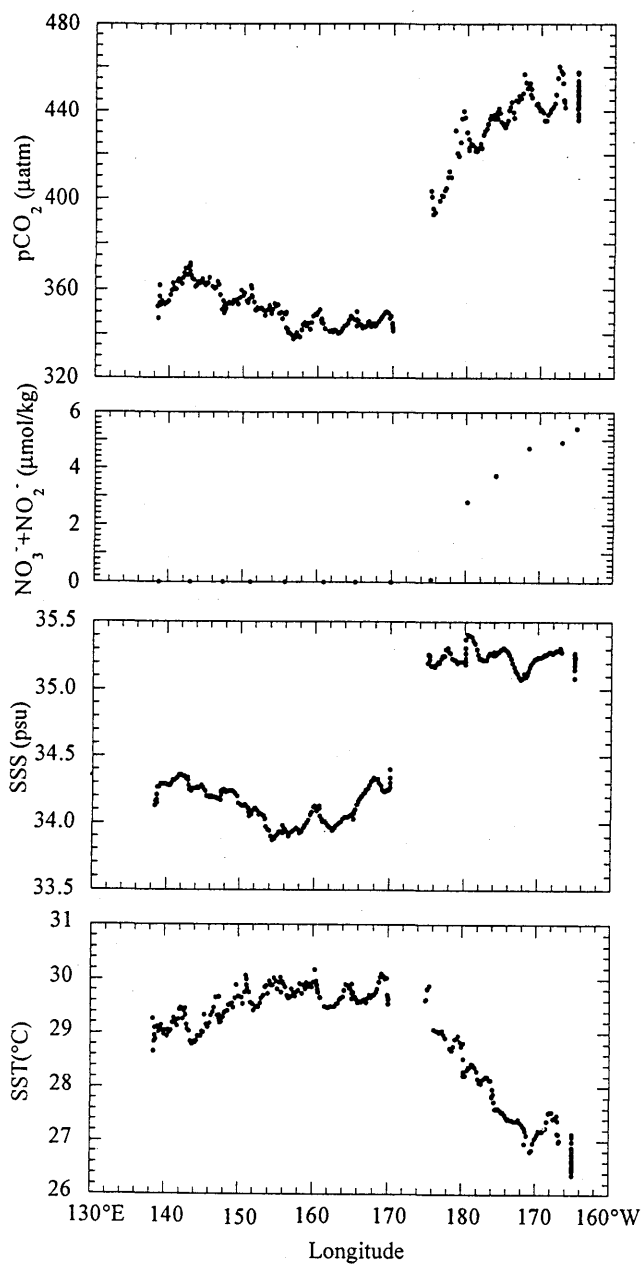


Fig. 96-7 Longitudinal distributions of pCO₂ (top), concentration of nitrate and nitrite (upper middle), SSS (lower middle), and SST (bottom) along equator for January-February 1994.

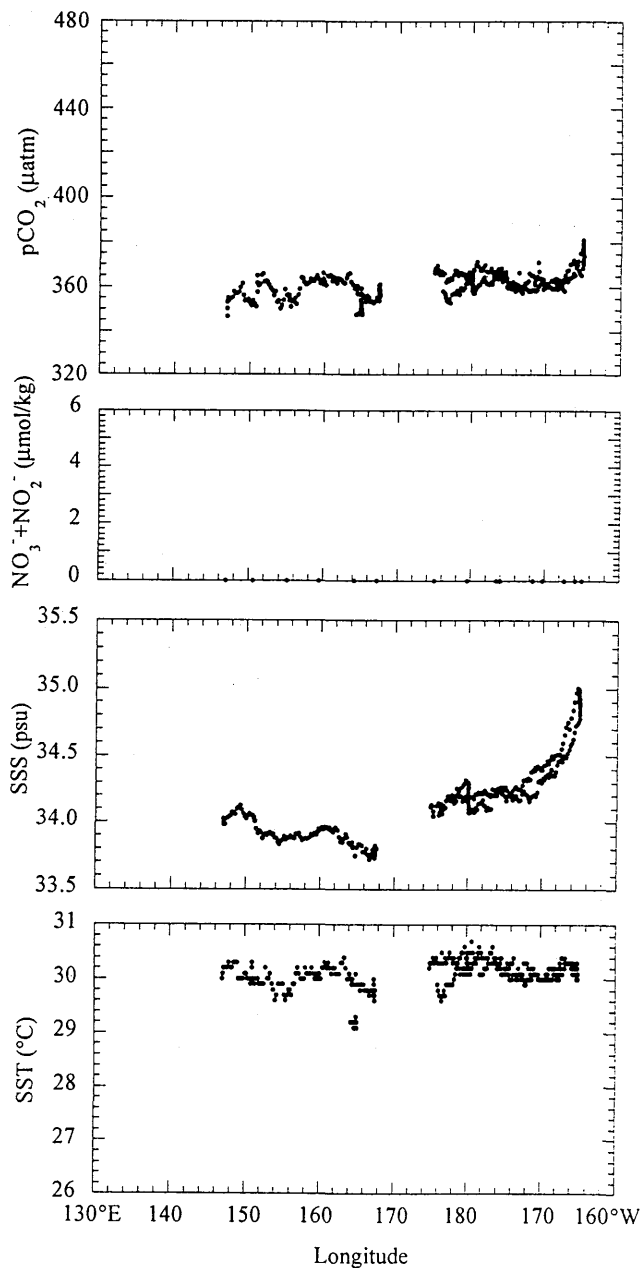


Fig. 96-8 Same as in Fig. 96-7 except for November-December 1994.

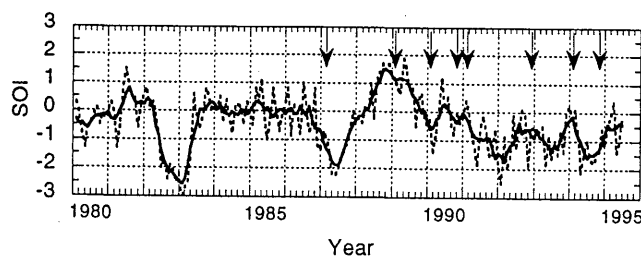


Fig. 96-9 SOI times series. Dotted line: monthly mean SOI; solid line: 5-month running mean. Arrows: pCO₂ observation times. Cruises in western and central equatorial Pacific were conducted January-February 1987, January-February 1989, January-February 1990, September-December 1990, January-February 1991, November-December 1992, January-February 1994, and November-December 1994.

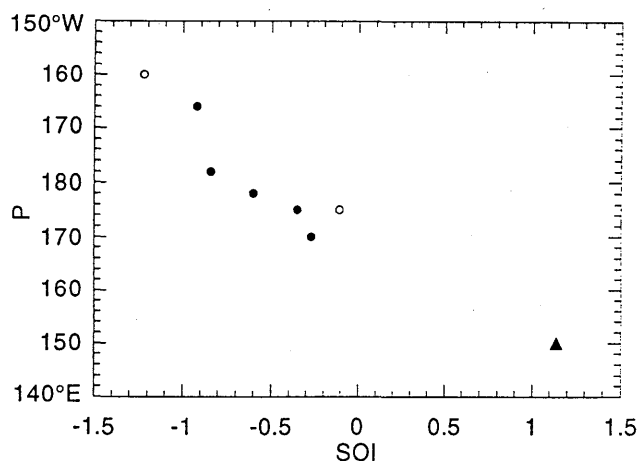


Fig. 96-10 Position (P) of abrupt change in pCO₂ and SOI. SOI during observation was calculated based on a 5-months running mean. pCO₂ data from September-October 1990 was not used because data around P (170°E-180°) was insufficient. Open circle: P along 5°S. During January-February 1989, P was estimated based on SST data (solid triangle).

2.3 Temporal and spatial variations in atmospheric and oceanic CO₂ in western North Pacific From 1990 to 1993: Possible link to 1991/92 ENSO event

Murata and Fushimi (1996)

Murata and Fushimi (1996) presented the results of atmospheric and oceanic CO₂ observations conducted by the JMA at 137°E in the western North Pacific for 1990 - 1993, covering an ENSO event (onset: spring 1991; disappearance: summer 1992) (Fig. 96-11). The atmospheric CO₂ concentration over the region south of 30°N increased drastically between 1990 and 1991 during winter (4.0 ppmv) and summer (4.5 ppmv), although values are not seasonally adjusted. Over the other two years of observation, growth rates were smaller or even negative (Figs. 96-12 and 96-13).

Oceanic CO₂, expressed in units of the mole fraction (ppmv) in dry air equilibrated with seawater, significantly increased, especially in low latitudes during both seasons of 1991 - 1993, compared to 1990 (Fig. 96-14). Oceanic CO₂, normalized at a constant temperature, also significantly increased, with larger magnitudes for winter and smaller for summer. This implies that increased summer oceanic CO₂ results mostly from changes in surface seawater temperature, while for that in winter, other factors, unknown at present, are more related to increased oceanic CO₂.

Calculated ΔpCO_2 and CO₂ flux at the air-sea interface reveal that in winter, the region north for 10°N acts

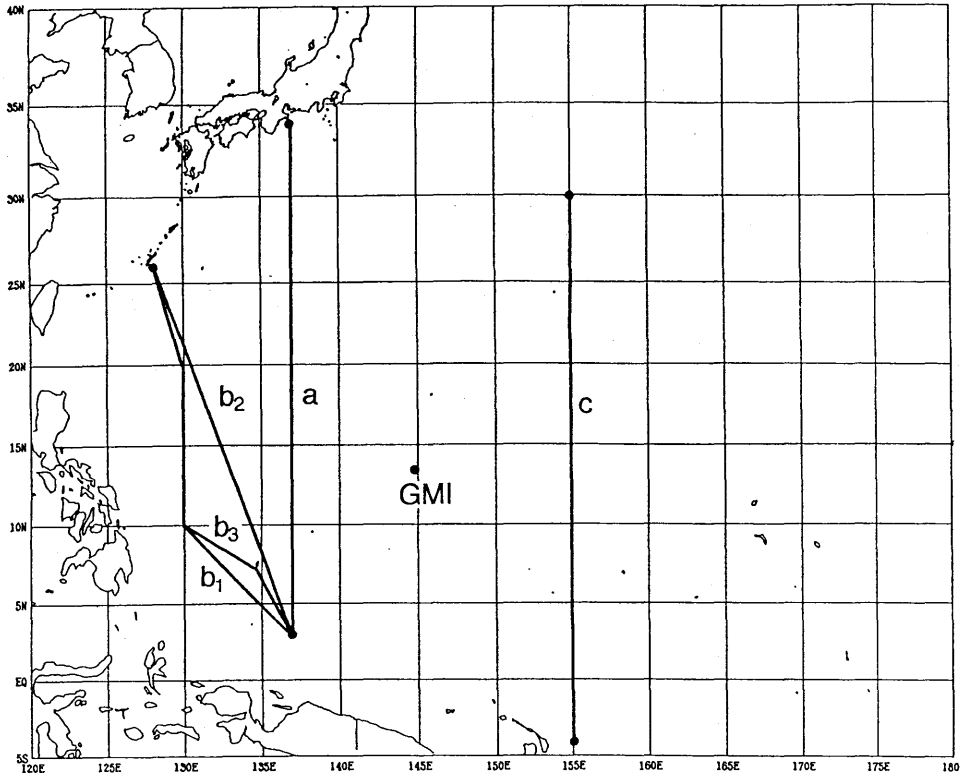


Fig. 96-11 Location of observational lines indicated as a 137°E, b_{1-3} lines west of 137°E, and c 155°E. The NOAA/CMDL GMI site (Guam, 13°26'N, 144°47'E) is also indicated.

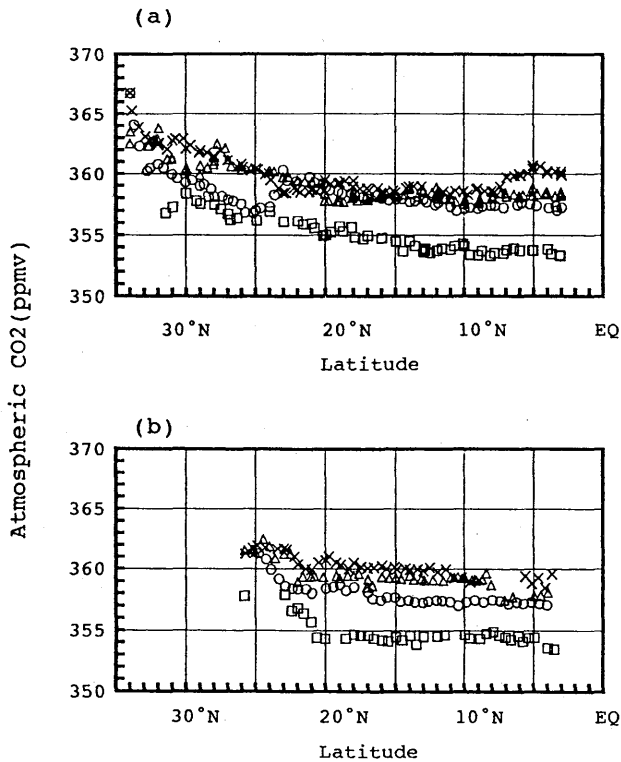


Fig. 96-12 Latitudinal distributions of atmospheric CO₂ during winter from 1990 to 1993, for (a) observational line along 137°E and (b) lines west of 137°E. Letters at upper left of panels correspond to observational lines in Fig. 96-11. Squares: 1990; circles: 1991; triangles: 1992; crosses: 1993.

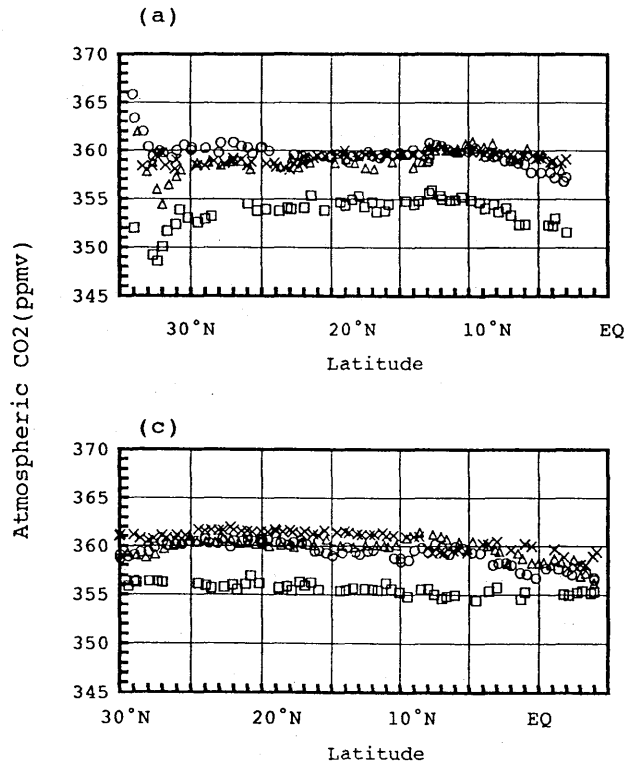


Fig. 96-13 Same as in Fig. 96-12 except for (a) observational line along 137°E and (c) that along 155°E during summer.

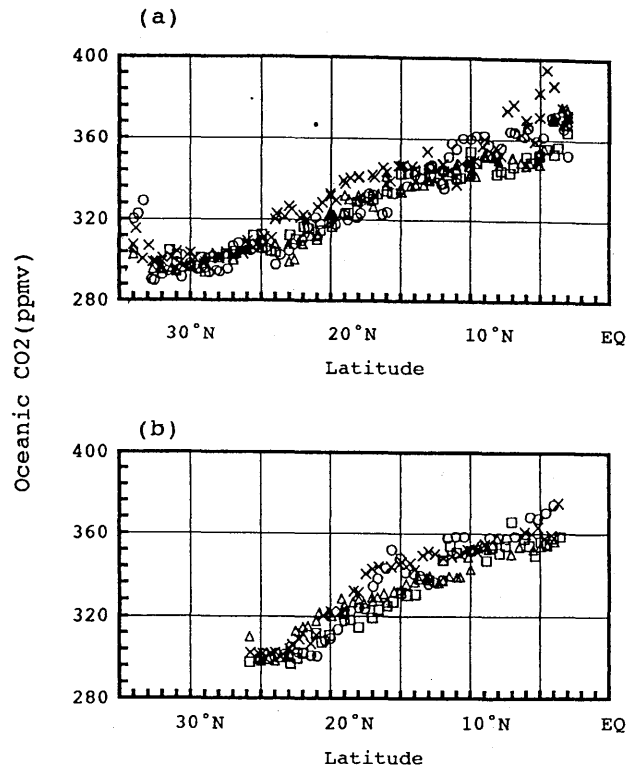


Fig. 96-14 Same as in Fig. 96-12 except for oceanic CO₂.

as a sink for CO₂, with a maximum net flux of $\sim -10.0 \text{ mmol} \cdot \text{m}^{-2} \cdot \text{d}^{-1}$. The region south of 10°N, however, at times becomes a weak source of CO₂, with a maximum net flux of $2.4 \text{ mmol} \cdot \text{m}^{-2} \cdot \text{d}^{-1}$. In summer, the western North Pacific becomes a weak source or is almost in equilibrium with atmospheric CO₂.

The increase in winter oceanic CO₂ or $\Delta p\text{CO}_2$, related to the 1991/92 ENSO event, is not as distinct as in the 1982/83 ENSO event, although lower temperatures and higher salinity in surface seawater were commonly found during both events. The response of CO₂ flux in the tropical western North Pacific to the 1991/92 ENSO event was rather small compared to the magnitude of rate changes obtained in previous results for the central or eastern tropical Pacific.

2.4 Atmospheric methane over North Pacific from 1987 to 1993

Matsueda, Inoue, Ishii, and Nogi (1996)

Atmospheric methane is known as an important greenhouse gas that influences the radiative balance and climate of the earth. Methane has accumulated in the atmosphere since the Industrial Revolution, but it is known that the recent global rate of increase shows large interannual variations in both hemispheres. Such growth rate variations are caused by a change in the relative strength between sources and sinks, but a particular cause cannot be quantitatively identified at the moment. A long-term record of atmospheric methane measurements is necessary to better understand recent growth rate variation.

Matsueda *et al.* (1996) continued to collect air samples over the western North Pacific region and measured atmospheric methane mixing ratios during winter from 1987 to 1993 to extend their methane record since 1978 (Matsueda *et al.*, 1992) (Fig. 96-15). The meridional distribution of methane showed a yearly north-to-south gradient from midlatitudes to the equator (Fig. 96-16). A sharp mixing ratio gradient often appeared at the boundary between the winter monsoon and trade wind regions around 20°N. No significant longitudinal gradient

was found during winter, although methane levels along the equator showed a large difference between the western and eastern Pacific.

The overall methane increase rate in the western Pacific was estimated at 13 ppb/yr based on the long-term record for 15 years from 1978 to 1993. This record indicates that the methane growth rate over this Pacific region gradually slowed until 1990, followed by no significant increase in the 1990s. The overall deceleration of the growth rate was more rapid in the middle latitudinal zone (20°N - 30°N) than in the lower latitudinal zone (3°N - 20°N) (Fig. 96-17a). This latitudinal difference suggests a rapid reduction of methane emission from continent. The methane growth rate showed an interannual variation with an increasing trend around 1983 and 1987, roughly related to El Niño events (Fig. 96-17b). The methane growth rate thus appears to have been affected by a change in interhemispheric transport due to the ENSO events.

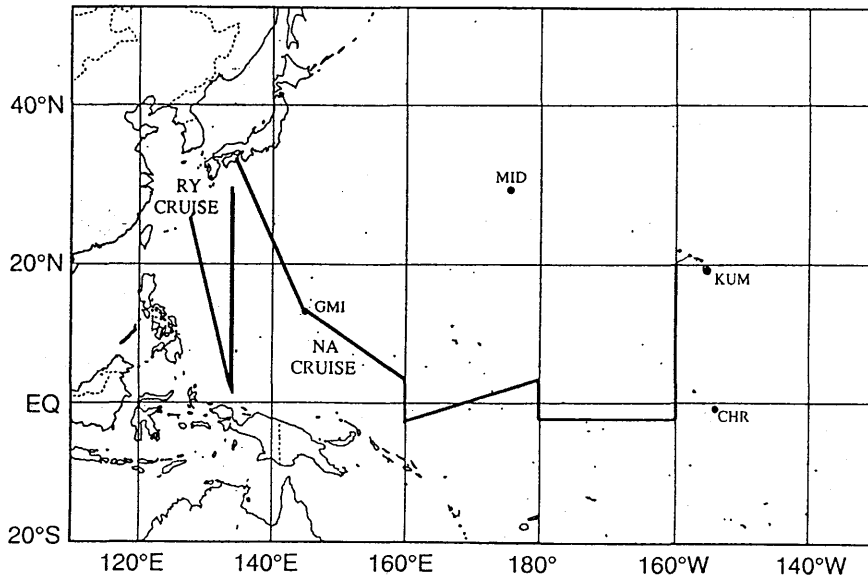


Fig. 96-15 Tracks of R/V *Ryofu Maru* (RY) and R/V *Natsushima* (NA) during January-February 1987. The sampling area of NA cruises was almost the same in 1989, 1990, and 1991, although tracks in these years were slightly different from that used in 1987.

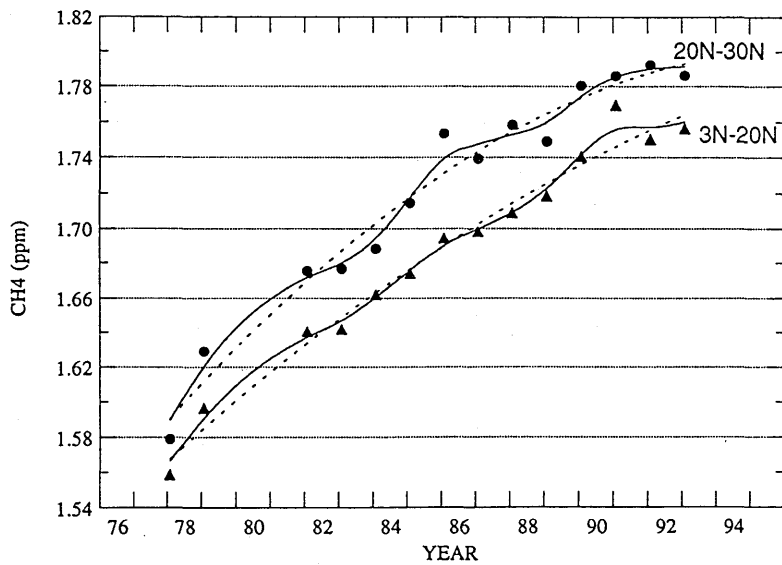


Fig. 96-16 Averaged methane mixing ratio in middle (20°N-30°N) and lower (3°N-20°N) latitudinal zones along 137°E in western Pacific from 1978 to 1993. Dashed lines: quadratic equation $f(t)$; solid lines: function $F(t)$; fitted to averaged data.

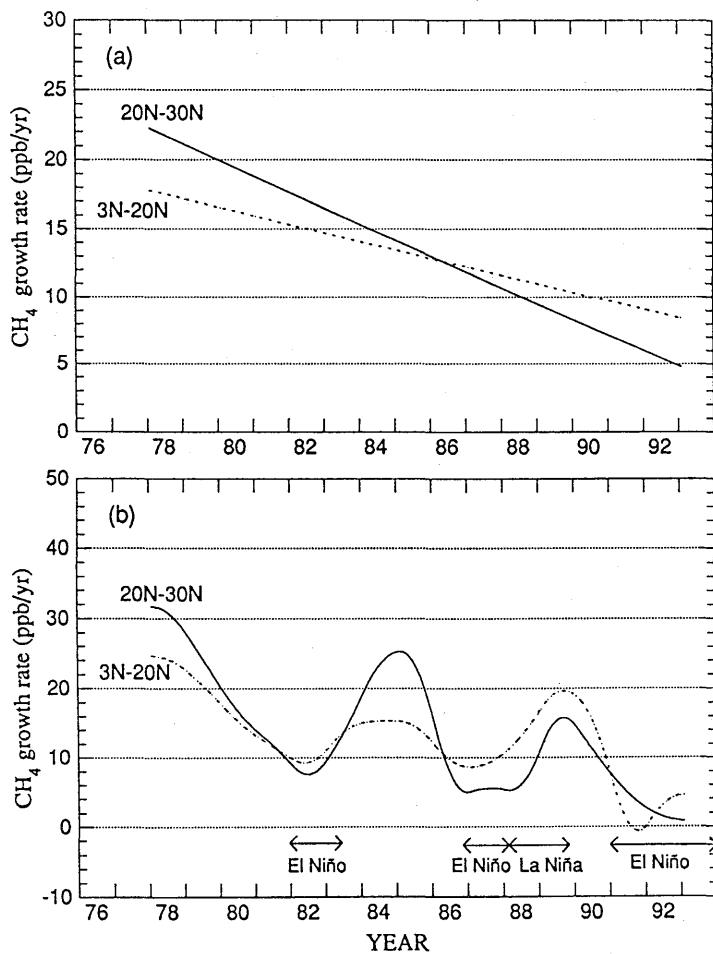


Fig. 96-17 Growth rate variations of atmospheric methane in middle (20°N-30°N) and lower (3°N-20°N) latitudinal zones along 137°E in western North Pacific from 1978 to 1993. (a) Overall trends and (b) interannual variation of growth rate were obtained by derivatives of $f(t)$ and $F(t)$ (Fig. 96-16).